Abdominal Radiology


Published online: 17 July 2018

Abdom Radiol (2019) 44:209–217
https://doi.org/10.1007/s00261-018-1703-0

# Magnetic resonance imaging findings of renal cell carcinoma associated with Xp11.2 translocation/TFE3 gene fusion in adults: a pilot study

Chenchen Dai,[1,2,3] Ruofan Sheng,[1,2,3] Yuqin Ding,[1,2,3] Minglei Yang,[4] Jun Hou,[5] and Jianjun Zhou[1,2,3]

[1]Department of Radiology, Zhongshan Hospital, Fudan University, No 180, Fenglin Road, Xuhui District, Shanghai 200032, China
[2]Shanghai Institute of Medical Imaging, No 180, Fenglin Road, Xuhui District, Shanghai 200032, China
[3]Department of Medical Imaging, Shanghai Medical College, Fudan University, No 220, Handan Road, Yangpu District, Shanghai 200032, China
[4]Siemems Healthineers, No 278 Zhouzhu Road, Pudong New District, Shanghai 200032, China
[5]Department of Pathology, Zhongshan Hospital, Fudan University, No 180, Fenglin Road, Xuhui District, Shanghai 200032, China

## Abstract

*Purpose:* The purpose of the study was to retrospectively analyze MRI findings of renal cell carcinoma associated with Xp11.2 translocation/TFE3 gene fusion (Xp11.2/TFE RCC) in adults.
*Methods:* Sixteen patients with Xp11.2/TFE RCC were reviewed retrospectively. The clinical characteristics and imaging features were assessed and then compared between metastatic and non-metastatic subgroups.
*Results:* The mean age at diagnosis was 47.4 (20–76) years. Seven (44 %) patients were men, and nine (56 %) patients were women. The lesions predominantly exhibited an endophytic distribution ($n$ = 14, 88 %) with a capsule ($n$ = 16, 100 %), accompanied by solid and cystic patterns ($n$ = 12, 75%) and hemorrhage ($n$ = 11, 69 %). The tumors prevalently appeared hyper- to isointense on T1WI ($n$ = 14, 88 %), hypointense on T2WI ($n$ = 13, 81 %), and hyperintense on DWI ($n$ = 16, 100 %) with a lower ADC ($P < 0.001$) than that of the surrounding tissue. The tumors were less enhanced than the normal renal cortex in all phases with a prolonged enhancement pattern ($P \leq 0.001$). In addition, six patients (38 %) developed recurrence or metastases. The RCCs with metastases showed an irregular shape ($P$ = 0.013), an incomplete capsule ($P$ = 0.018), heterogeneous solid-cystic patterns ($P$ = 0.034), and hemorrhage ($P$ = 0.037) than non-metastatic subgroups.
*Conclusions:* MRI provides valuable information for the diagnosis of adult Xp11.2/TFE RCCs. Features including irregular shape, incomplete capsule, mixed solid-cystic pattern, and hemorrhage may indicate the occurrence of recurrence or metastases.

**Key words:** Renal cell carcinoma—Adult—Magnetic resonance imaging—Diagnosis—Prognosis

**Abbreviation**

| | |
|---|---|
| WHO | World Health Organization |
| RCC | Renal cell carcinoma |
| Xp11.2/TFERCC | Xp11.2 Translocation/TFE3 gene fusion renal cell carcinoma |
| CT | Computed tomography |
| PET-CT | Positron emission tomography-computed tomography |
| DWI | Diffusion-weighted imaging |
| ADC | Apparent diffusion coefficient |
| IHC | Immunohistochemistry |
| FISH | Fluorescence in situ hybridization |
| ROI | Region of interest |

Renal cell carcinoma associated with Xp11.2 translocation/TFE3 gene fusion (Xp11.2/TFE RCC) is defined by different translocations involving chromosome Xp11.2,

*Correspondence to:* Jianjun Zhou; *email:* zhoujianjunzs@126.com

all resulting in gene fusions involving the TFE3 gene, and was first identified as a separate entity by the 2004 World Health Organization [1]. Xp11.2/TFE RCC is a rare subtype of RCC primarily affecting children and young adults, especially women [2]. However, due to its low incidence, adult tumor is seriously underestimated in the clinic [3, 4]. Researchers suggested that adult Xp11.2/TFE RCC has a high degree of invasiveness with a rapid disease course and has a poor prognosis than the disease in children [5, 6]. Therefore, a more in-depth understanding of this tumor in adult is clinically relevant.

Until now, most studies have focused on imaging findings by computed tomography (CT) in children or young adults [7–11]. The advantages of MRI are its sensitive detection of details and the ability to provide multi-sequence information, such as diffusion-weighted imaging (DWI). However, MR imaging features of Xp11.2/TFE RCC have been published in only a few case reports and have not yet been fully evaluated due to the small number of cases [6, 12, 13]. Thus, the aim of this study was to further investigate the MR imaging findings of Xp11.2/TFE RCC in adult patients.

## Materials and methods

### *Patients*

This retrospective study was approved by the institutional review board, and informed consent was waived. Thirty-three adult patients with Xp11.2/TFE RCC from July 2014 to August 2016 were selected by searching the pathologic databases at our institution. Thirteen cases were excluded due to the availability of only CT images or the unavailability of pretreatment dynamic contrast-enhanced MR images. Three cases were excluded because the lesions did not undergo immunohistochemistry (IHC) or fluorescence in situ hybridization (FISH) analysis. In addition, one case with a lesion diameter smaller than 1 cm was excluded to avoid potential confounding of partial volume averaging. The remaining 16 lesions in 16 patients were included in our study.

### *MR examination*

All MR images were acquired using a 1.5 T MR system (Magnetom Aera; Siemens Healthcare, Erlangen, Germany) with an 18-channel body phase array coil. The conventional MR protocol used in this study included a transverse respiratory-navigated, T2-weighted, fat-suppressed turbo spin-echo sequence (TR/TE = 3220/96 ms; section thickness, 5 mm; and intersection gap, 1 mm; matrix, 320 × 224 matrix) and a transverse T1-weighted in-phase and opposed-phase gradient echo (TR/TE = 6.9/4.76 ms (in-phase); TR/TE = 6.9/2.38 ms (opposed-phase); section thickness, 3 mm; intersection gap, 0.6 mm; matrix, 320 × 240). DWI was required with a transverse single-shot spin-echo echo-planar sequence (TR/TE = 5100/70 ms; section thickness, 5 mm; intersection gap, 1 mm; matrix, 128 × 128) with $b$ values of 0 and 500 s/mm$^2$. Dynamic imaging was performed once before and three times after intravenous administration of gadopentetate dimeglumine (Magnevist; Bayer HealthCare, Germany) using a transverse breath-hold T1-weighted 3-dimensional volumetric interpolated body examination sequence (TR/TE = 4.36/1.93 ms; section thickness, 3 mm; intersection gap, 0.6 mm; matrix, 228 × 216). Gadopentetate dimeglumine was administered at a dose of 0.1 mmol/kg and at a rate of 2 ml/s followed by a 20-ml saline flush using a power injector (Spectris; Medrad, Pittsburgh, PA, USA). Acquisitions were performed at 20~25, 80~90, and 160~180 s after contrast administration during the corticomedullary, nephrographic, and delayed phases, respectively.

### *MR image analysis*

Two radiologists (C.C.D. and J.J.Z., with 4 and 28 years of experience in genitourinary imaging, respectively) performed imaging analysis and ultimately achieved consensus interpretation using PACS technology (Pathspeed; GE Medical Systems Integrated Imaging Solutions, Prospect, IL, USA). The reviewers evaluated the following characteristics of each renal mass: tumor size (maximal diameter), epicenter (endophytic vs. exophytic, according to the location of the lesion center within the outline of the kidney), shape (regular vs. irregular, a regular shape was characterized as round or oval. Irregular shapes included a roughly round or oval tumor with focal protrusions and lobulated and infiltrative grow patterns), angular interface (renal masses having a tapered or an angled interface within the parenchyma), capsule (hypointense on T2WI and delayed enhancement, complete vs. incomplete), composition (solid, predominantly solid, mixed solid and cystic, and predominantly cystic), hemorrhage (high signal intensity on unenhanced fat-saturated T1W images), and fat (diagnosed if there is signal drop on opposed-phase relative to in-phase).

T1WI, T2WI, and DWI images were qualitatively assessed on a workstation. Mean apparent diffusion coefficient (ADC) values of the tumor and renal cortex were obtained from the ADC maps for each patient. Tumor enhancement was evaluated by the enhancement pattern and SI changes. The enhancement pattern was defined by enhancement heterogeneity, and values were measured using the region of interest (ROI). For heterogeneous tumors, ROIs were drawn on apparently enhancing solid component within the tumor as much as possible, avoiding the area of cystic degeneration, necrosis, and hemorrhage via comparison with T1- and T2-weighted images. For homogeneous tumors, the ROI encompassed the entire lesion. The ROI of the renal cortex was placed within the ipsilateral kidney uninvolved by the tumor. Each ROI was drawn twice by one

radiologist, and the average was used for analysis. SI changes = $[(SI_{post} - SI_{pre})/SI_{pre}] \times 100$, where $SI_{post}$ is the SI of the ROI in contrast-enhanced phase images and $SI_{pre}$ is the SI of the ROI in unenhanced images.

### *Pathological analysis*

All pathologic analyses were performed by a pathologist (J.H.) with 13 years of experience. Pathological features and IHC staining histological diagnoses, including TFE3 immunostaining, were routinely performed. However, there was a fairly high false-positive rate when detecting the TFE3 protein by IHC [14]. Recently, a TFE3 break-apart FISH assay was evaluated to fully confirm the diagnosis of Xp11.2/TFE RCC [15]. The co-localization of red and green signals in tumor nuclei was regarded as negative. A split signal in more than 10% of tumor nuclei was regarded as positive for TFE3 rearrangement [16].

### *Follow-up analysis*

Another radiologist (Y.Q.D.) collected follow-up information by using institutional electronic medical records, which was blinded to C.C.D. and J.J.Z. Patient characteristics and imaging features, including age, sex, morphologic features, signal features, enhancement, enlarged regional lymph nodes, and vascular invasion, were compared between the non-metastatic and metastatic groups (local recurrence or distant metastasis). The follow-up time interval was defined as the interval from the initial imaging study to the last time that CT, MR, or PET-CT examination was performed in our institution. The tumor growth rate was also calculated using measured changes in the maximum axial diameter per year (only for patients who had at least two imaging studies obtained at least 6 months apart).

### *Statistical analysis*

Continuous data are expressed as mean values and were compared using Student's $t$ test or repeated-measures ANOVA (i.e., age, size, percentage SI changes, or ADC value). Specific imaging features were recorded by count data and were compared by Fisher's exact test. All statistical analyses were performed using SPSS 20.0 (Chicago, IL, USA). $P < 0.05$ was considered statistically significant.

## Results

### *Patient characteristics*

Clinical data of 16 cases of Xp11.2/TFE RCC are presented in Table 1. The mean age at diagnosis was 47.4 years (range 20–76 years). Seven (44 %) men and nine (56 %) women were included. The time interval from MRI to surgical treatment was 2 weeks or less.

### *Tumor characteristics*

The characteristics of Xp11.2/TFE RCC are summarized in Table 2. The average diameter was 5.0 cm (range 1.7–14.6 cm). Tumor epicenters were endophytic

**Table 1.** Clinical data of 16 cases of Xp11.2/TFE RCC

| No. | Age /sex/laterality | Size (cm) | Symptoms | Surgical approaches | Follow-up (months) | Recurrence or metastases |
|---|---|---|---|---|---|---|
| 1 | 60/F/L | 3.2 | No | ORN | 12 | No |
| 2 | 30/F/R | 4.1 | No | LNSN | 36 | No |
| 3 | 62/F/L | 3.3 | No | ONSN | 30 | No |
| 4 | 76/M/L | 2.9 | No | ONSN | 63 | No |
| 5 | 59/F/R | 2.4 | No | ONSN | 14 | No |
| 6 | 58/M/L | 2.9 | No | LNSN | – | No |
| 7 | 52/F/R | 4.8 | Hematuria, flank pain | ORN | 15 | No |
| 8 | 76/M/L | 1.7 | No | ONSN | 48 | No |
| 9 | 27/F/R | 5.2 | No | ONSN | 11 | No |
| 10 | 29/M/R | 1.9 | Hematuria | ONSN | 38 | No |
| 11 | 20/F/R | 6.4 | Flank pain | ORN | 12 | Right adrenal glands, liver, lumbar (12 months)[a] |
| 12 | 31/M/L | 2.6 | No | LNSN | 23 | Retroperitoneal space (15 months) |
| 13 | 39/F/L | 4.8 | Flank pain | Needle biopsy | – | Retroperitoneal space, liver (0 month) |
| 14 | 52/M/L | 7.0 | Hematuria, flank pain | ORN | 7 | Nephrectomy bed (7 months) |
| 15 | 26/F/L | 14.6 | Hematuria | ORN | 12 | Retroperitoneal space, nephrectomy bed (12 months) |
| 16 | 61/M/R | 12.6 | Palpable mass | ORN | 2 | Lung (0 month) |

[a]Data in parentheses were the time of recurrence or metastases founded
M, Male; F, Female; L, Left; R, Right; ORN, Open radical nephrectomy; LRN, Laparoscopic radical nephrectomy; ONSN, Open nephron-sparing nephrectomy; LNSN, laparoscopic nephron-sparing nephrectomy

**Table 2.** Patient and tumor characteristics of Xp11.2/TFE RCC

| Tumor feature | Total | Non-metastatic | Metastatic | *P* |
|---|---|---|---|---|
| No. of tumors[a] | 16 (100) | 10 (63) | 6 (38) | – |
| Age (years, range)[b] | 47.4 (20–76) | 52.9 (27–76) | 38.2 (20–61) | 0.125[c] |
| Sex (M:F) | 7 (44):9 (56) | 4 (40):6 (60) | 3 (50):3 (50) | 0.696[d] |
| Size (cm, range)[b] | 5.0 (1.7–14.6) | 3.2 (1.7–5.2) | 8.0 (2.6–14.6) | 0.053[c] |
| Laterality (L:R) | 9 (56):7 (44) | 5 (50):5 (50) | 4 (67):2 (33) | 0.515[d] |
| Symptoms(Y:N) | 7 (44):9 (56) | 2 (20):8 (80) | 5 (83):1 (17) | 0.013[d] |
| Follow-up (months, range)[b] | 23 (2–63) | 30 (11–63) | 11 (2–23) | – |
| Endophytic epicenter (Y:N) | 14 (88):2 (13) | 9 (90):1 (10) | 5 (83):1 (17) | 0.696[d] |
| Shape (regular:irregular) | 9 (56):7 (44) | 8 (80):2 (20) | 1 (17):5 (83) | 0.013[d] |
| Angular interface (Y:N) | 6 (38):10 (63) | 5 (50):5 (50) | 1 (17):5 (83) | 0.182[d] |
| Capsule (complete:incomplete) | 11 (69):5 (31) | 9 (90):1 (10) | 2 (33):4 (67) | 0.018[d] |
| Solid and cystic pattern | | | | 0.034[d] |
| Solid | 4 (25) | 4 (40) | 0 (0) | |
| Predominantly solid | 7 (44) | 4 (40) | 3 (50) | |
| Mixed solid and cystic | 3 (19) | 0 (0) | 3 (50) | |
| Predominantly cystic | 2 (13) | 2 (20) | 0 (0) | |
| Hemorrhage (Y:N) | 11 (69):5 (31) | 5 (50):5 (50) | 6 (100):0 (0) | 0.037[d] |
| Microscopic fat (Y:N) | 0 (0):16 (100) | 0 (0):10 (100) | 0 (0):6 (100) | – |
| Enlarged lymph nodes (Y:N) | 3 (19):13 (81) | 1 (10):9 (90) | 2 (33):4 (67) | 0.247[d] |
| Vascular invasion (Y:N) | 2 (13):14 (88) | 0 (0):10 (100) | 2 (33):4 (67) | 0.051[d] |
| T1 unenhanced signal | | | | |
| Hypo-/iso-/hyperintense | 2 (13)/5 (31)/9 (56) | 2 (20)/3 (30)/5 (50) | 0 (0)/2 (33)/4 (67) | 0.497[d] |
| T2 signal | | | | |
| Heterogeneity (Y:N) | 14 (88):2 (13) | 8 (80):2 (20) | 6 (100):0 (0) | 0.242[d] |
| Hypo-/iso-/hyperintense | 13 (81)/1 (6)/2 (13) | 7 (70)/1 (10)/2 (20) | 6 (100)/0 (0)/0 (0) | 0.330[d] |
| Hyperintense on DWI (Y:N) | 16 (100):0(0) | 10 (100):0 (0) | 6 (100):0 (0) | – |
| Enhancement heterogeneity (Y:N) | 7 (44):9 (56) | 2 (20):8 (80) | 5 (83):1 (17) | 0.013[d] |

[a]Data are numbers of patients, with percentages in parentheses
[b]Data are expressed as medians, with ranges in parentheses
[c]From an independent sample *t*-test to compare continuous variables between the non-metastatic and metastatic groups
[d]From Fisher's exact test to compare count data between the non-metastatic and metastatic groups

($n$ = 14, 88 %) with a capsule ($n$ = 16, 100 %) (Figs. 1A, 4E). Six (38 %) tumors presented an angular interface with the renal parenchyma (Figs. 1D, 4C, D). Seventy-five percent ($n$ = 12) of Xp11.2/TFE RCCs presented solid-cystic degeneration, 69 % ($n$ = 11) with hemorrhage, and no tumor ($n$ = 0) with fat.

The signal features on T1WI and T2WI are shown in Table 2. Eighty-eight percent ($n$ = 14) of tumors showed a heterogeneous appearance. On DWI, all tumors showed hyperintensity to varying degrees. The mean tumor ADC value was significantly lower than that of the surrounding renal cortex ($1.52 \pm 0.61$) $\times 10^{-3}$ vs. ($2.36 \pm 0.30$) $\times 10^{-3}$ mm$^2$/s, $t = -4.558$, $P = 0.000$) (Fig. 1B). After contrast, the mean percentage SI changes in the tumor and renal cortex were (111 ± 79)% and (212 ± 79)% at the corticomedullary phase, (136 ± 65)% and (264 ± 82)% at the nephrographic phase, and (132 ± 67)% and (256 ± 78)% at the excretory phase, respectively. Each phase showed a significant difference between the tumor and the cortex (corticomedullary, $Z = -3.242$, $P = 0.001$; nephrographic, $Z = -3.619$, $P = 0.000$; excretory, $t = -4.828$, $P = 0.000$). Dynamic percentage SI change curves are displayed in Fig. 2.

## *Histopathology findings*

Microscopically, tumor cells were predominantly polygonal with voluminous eosinophilic or nuclear cytoplasm and were arranged with a papillary or nested architecture (Fig. 3A). Forty-three percent of lesions ($n$ = 7) had distinct psammoma bodies. Strong TFE3 protein expression (Fig. 3B) and a positive FISH assay results (Fig. 3C) were obtained in all cases.

## *Imaging Follow-up*

Imaging follow-up information was available for 14 out of 16 patients (88%), and the median follow-up time was 23 months (range 2–63 months) (Tables 1, 2). Six (38 %) patients developed locally recurrent or distant metastatic disease, the interval to metastasis was about 8 months (range 0–15 months) (Tables 1, 2). In addition, we reviewed sequential CT or MRI examinations for one patient, and the growth rate was approximately 0.7 cm per year over a four-year follow-up (Fig. 4).

Eighty-three percent ($n$ = 5) of patients with recurrence or metastases were associated with clinical symptoms, while 20% ($n$ = 2) non-metastatic patients had symptoms, and the difference was statistically significant

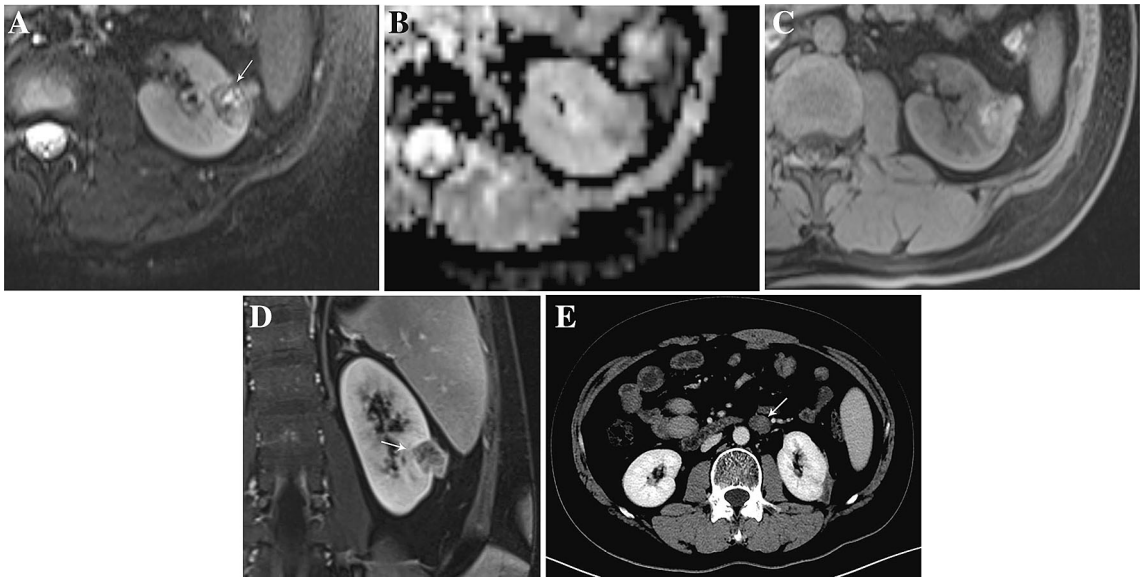


**Fig. 1.** A 31-year-old man with a 2.6-cm surgically proven Xp11.2/TFE RCC that was incidentally discovered. **A** Transverse T2-weighted image showed an irregular, slightly heterogeneous hypointense mass with an incomplete capsule (arrow). **B** ADC map showed hypointensity, and the ADC value was approximately $1.69 \times 10^{-3}$ $mm^2/s$. **C** Transverse T1-weighted image showed hyperintensity with extensive intratumoral hemorrhage. **D** Coronal delayed phase image showed the tumor center was within the outline of the kidney, and the lesions showed mild enhancement. Masses had a tapering, almost pyramidal interfacing with the renal parenchyma (arrow) and were surrounded by a clear, thickened capsule. **E** Transverse contrast-enhanced CT images through the upper abdomen obtained 15 months after **A** showed a new para-aortic node (arrow).

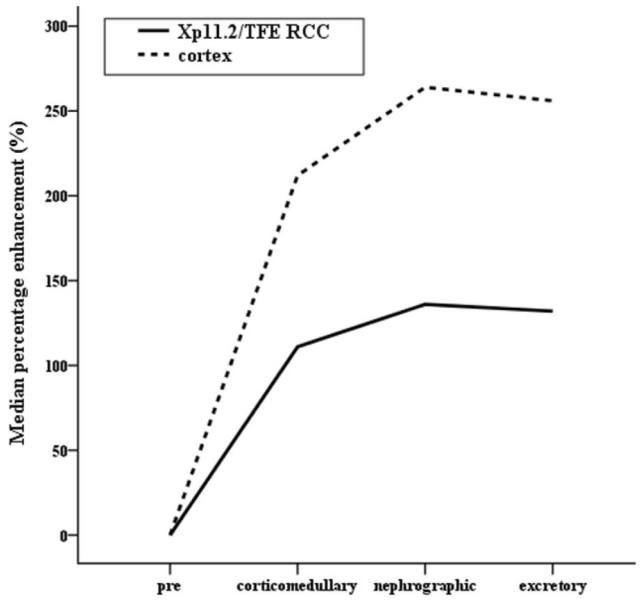


**Fig. 2.** Median percentage enhancement of Xp11.2/TFE RCC. Xp11.2/TFE RCC showed mild, prolonged enhancement after contrast agent administration. Tumors had significantly lower SI enhancement ratios than the cortex ($P < 0.05$) during the corticomedullary, nephrographic, and excretory phases.

($P = 0.013$). Comparing with non-metastatic subgroups, the primary renal tumors that had metastases exhibited an irregular shape ($P = 0.013$), incomplete capsule ($P = 0.018$), heterogeneous solid and cystic patterns ($P = 0.034$), and intratumor hemorrhage ($P = 0.037$) (Fig. 1). With the exception of heterogeneous enhancement ($P = 0.013$), there were no significant differences in enlarged regional lymph nodes, vascular invasion, signal intensity (on T1WI, T2WI, and DWI) and quantitative measurements (ADC value and enhancement) between the two groups ($P > 0.05$). In addition, no significant differences were found for patient age and tumor size ($P > 0.05$).

## Discussion

In this study, adult patients with Xp11.2/TFE RCC demonstrated no obvious association with age or sex, which differed from the predilection for individuals of a younger age and women reported in previous studies. Regional differences and our inclusion criteria of only adult patients may have resulted in this discrepancy. Our results showed that Xp11.2/TFE RCCs presented predominantly endophytic epicenters with a capsule, accompanied by a solid and cystic pattern and hemorrhage. An angular interface with the renal parenchyma was occasionally seen. Lesions prevalently appeared hyper- to isointense on T1WI, heterogeneously hypointense on T2WI, and hyperintense on DWI with lower ADC values than the surrounding renal cortex. The lesions showed mild, prolonged enhancement.

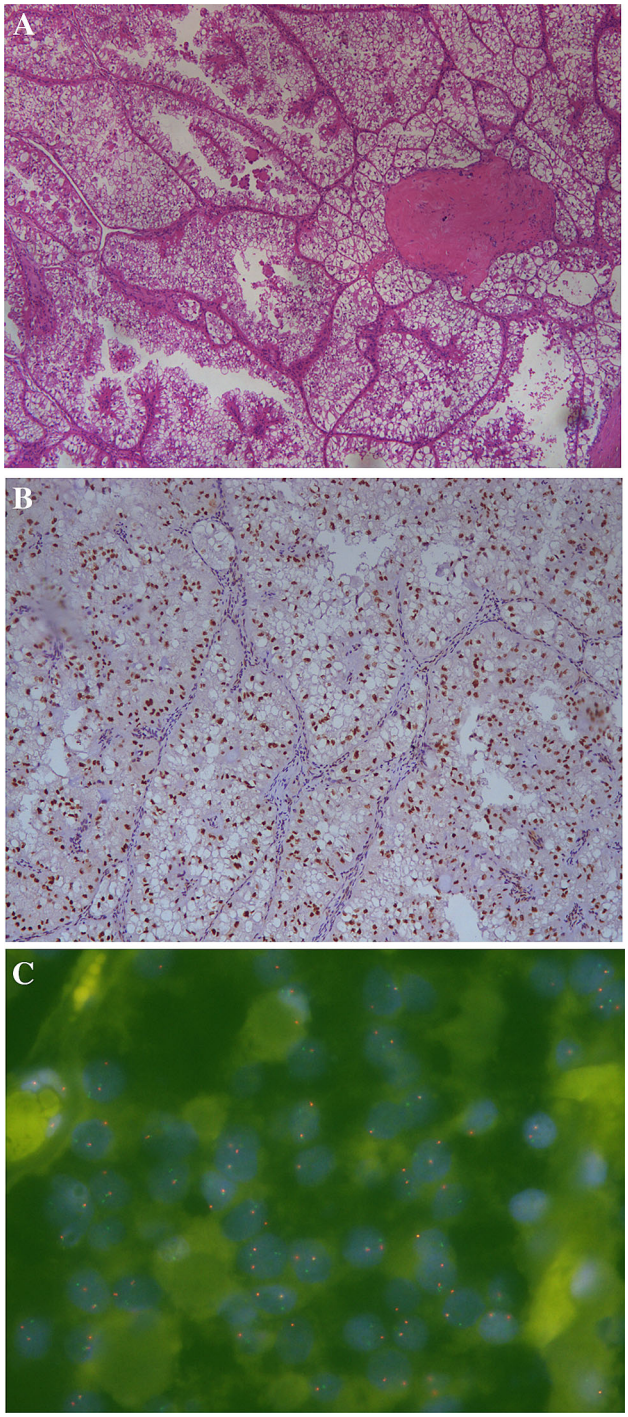


**Fig. 3.** A 38-year-old man with typical pathologic features of Xp11.2/TFE RCC. **A** Hematoxylin–eosin staining showed that the tumor cells were dense and arranged with a papillary or nested architecture (× 100). **B** Immunohistochemical staining showed diffuse, strong TFE3 protein expression in the nuclei (× 100). **C** Fluorescence in situ hybridization (FISH) showed separated red and green signals in more than 10% of tumor nuclei, which were considered positive for TFE3 rearrangement (× 1000).

MRI provides more information by detecting details with greater sensitivity and is useful for better characterization. In our study, all lesions had a thick capsule presenting hypointensity on T2WI and delayed enhancement. Comparable to the largest sample in the CT literature [11], only 76 % of cases (16/21) had a capsule sign. Notably, we preliminarily found that six cases had an angular interface with the renal parenchyma. Verma et al. [17] suggested that the presence of an angular interface with the renal parenchyma was a strong predictor of fat-poor angiomyolipoma. However, capsule was not often seen on fat-poor angiomyolipoma, which is helpful for distinguishing it from XP11.2/TFE RCC [17]. Additionally, two lesions presented as a unilocular cystic mass with intratumoral septations, exhibiting overlapping features with cystic RCC, a manifestation that has never previously been reported in the literature (Fig. 5).

In our study, Xp11.2/TFE RCC predominantly appeared heterogeneous hypointense on T2WI, consistent with prior studies [6, 13]. Heterogeneity is often assigned to cystic degeneration, necrosis, or hemorrhage [12]. Papillary architecture or hemorrhage is responsible for hypointensity on T2WI [18, 19]. In addition, most lesions appeared as hyperintense on DWI and showed significantly lower ADC values than the surrounding renal cortex, indicating markedly restricted diffusion among tumor tissues. At pathology, Xp11.2/TFE RCC was composed of dense cells with a papillary or nested architecture, and its compact tissue architecture limited water diffusion in the interstitial space. The ADC value in our study was similar to that of four cases reported by Razek et al. [20] [$(1.50 \pm 0.97) \times 10^{-3}$ $mm^2/s$]. However, with the exception of clear cell RCCs, many other renal tumors also show hypointensity on T2WI and restricted diffusion on DWI [18, 20, 21]. Thus, ancillary imaging features need to be considered for differentiation. For example, Xp11.2/TFE RCC contained more cystic components than papillary RCC [10, 22]; chromophobe RCC is always characteristic of homogeneity [23], and angiomyolipoma is often hypervascular [24]. On contrast-enhanced MRI, Wang et al. [25] suggested that Xp11.2/TFE RCCs are hypovascular tumors that show heterogeneous enhancement. Our results agree with these findings and go a step further by quantitative analysis—in particular, lesions showed mildly increasing attenuation in the corticomedullary phase with prolonged enhancement in the nephrographic and excretory phases, suggesting dynamic changes in the blood supply. In comparison, the third subtype, papillary RCCs, were also hypovascular and showed slight, prolonged enhancement [26], whereas papillary RCCs usually affect older men and tend to be in smaller size than Xp11.2/TFE RCCs [10, 22].

In our study, although there were no significant differences, we found that patients with metastatic disease

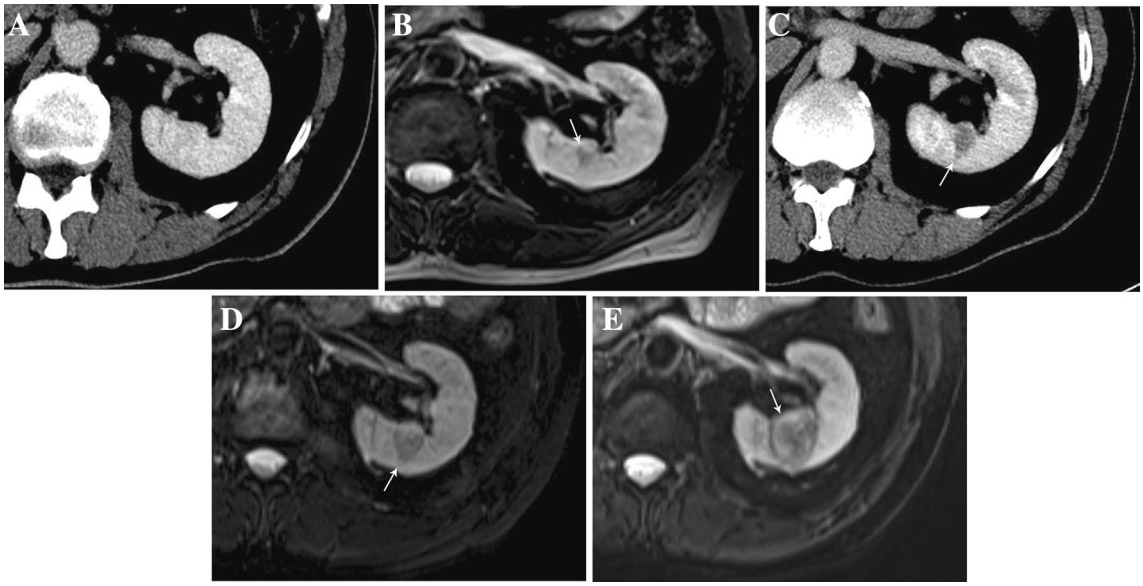


**Fig. 4.** A 76-year-old man with four-year follow-up. The tumor was relatively stable, and the growth rate was approximately 0.7 cm/year. **A** Axial CT contrast-enhanced image found no obvious mass in the left kidney in March 2012. **B** MR image showed a new, small mass (arrow) measuring 10.0 mm in June 2013. **C** CT image showed enlargement of the mass (19.0 mm) in January 2014, and the mass made a clear angular interface with the renal parenchyma (arrow). **D** Transverse T2-weighted image showed a homogeneous hypointense mass, measuring 19.2 mm, in January 2015 (arrow). **E** Transverse T2-weighted image revealed a slightly heterogeneous hypointense mass with complete capsule, measuring 29.0 mm, in June 2016 (arrow). The tumor was relatively stable and the growth rate was about 0.7 cm/year. The mass arised from the renal medulla and gradually became larger with growing up.

had a younger age than non-metastatic subgroups, similar to the result of Liu et al. [27] in which the age of advanced patients was about 35 years in all 34 cases, and this phenomenon needs to be verified with a larger sample. Combination with clinical manifestations is helpful for the diagnosis, but considering the non-specificity and overlaps, it is essential to further evaluate the imaging features. Although we did not identify any reliable signal intensity and enhancement performance that might permit the distinction of non-invasive and metastatic disease, morphological features were clues to the identification. According to our results, the primary tumors with metastases were more likely to have an irregular shape and incomplete capsule and more likely to show a mixed solid-cystic pattern and hemorrhage, as well as more likely to exhibit heterogeneous enhancement, than the non-metastatic group. In addition, we observed growth in one case with a four-year follow-up, and this non-invasive tumor was relatively stable in size. Egbert et al. [28] reported 0.5 cm/year for Type 1 papillary RCCs and 0.7 cm/year for Type 2, which were close to the growth rate of Xp11.2/TFE RCC (0.7 cm/year) in our study. Although this finding may not be generalized, it could provide us with some experiences in risk assessment and management decisions [29, 30].

The major limitations of our study were lack of qualitative and quantitative comparisons with other renal masses as it may provide great value for clinical work-up. According to our descriptive comparisons in the above text and previous literatures [4, 7, 10, 20, 22], its certain features, such as affected population, tumor location, hypo-vascularity, and the ADC value, make it not very difficult to distinguish Xp11.2/TFE RCCs from others. Of course, further study is needed to make persuasive comparisons. Second, this study was limited by its small sample size and the nature of retrospective study may introduce inherent selection and verification biases. However, Xp11.2/TFE RCC is rare and the number of cases in our study was still larger than that of any other report on MR imaging findings [6, 12, 13]. Third, calcification may be one of the useful signs and 19% (11/57) Xp11.2/TFE RCC contained calcification on CT [7–11], but that poorly detected by MRI. The joint use of CT and MRI could help radiologists to identify.

In summary, Xp11.2/TFE RCCs demonstrated no obvious associations with age or sex in adult patients. The dominant lesions exhibited an endophytic distribution with a thickened capsule, accompanied by solid-cystic patterns and hemorrhage. In terms of signal features, the tumors prevalently appeared hyper- to isointense on T1WI and heterogeneously hypointense on T2WI and exhibited restricted diffusion on DWI. After contrast, the lesions showed a mild, prolonged enhancement pattern. Furthermore, the Xp11.2/TFE RCCs with metastases are more likely to present an irregular shape, an incomplete capsule, and a solid-cystic

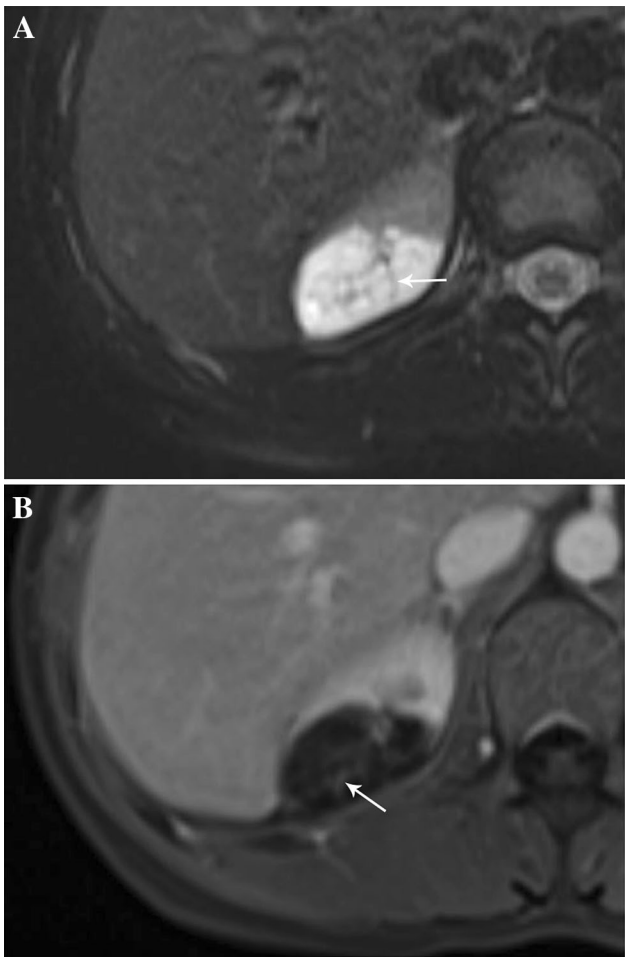


**Fig. 5.** A 30-year-old woman with "atypical" Xp11.2/TFE RCC. **A** Transverse T2-weighted image showed a hyperintense cystic mass with hypointense septations (arrow). **B** Transverse nephrographic phase image showed unsmooth, enhanced septations (arrow).

pattern and hemorrhage than the non-metastatic subgroup.

**Acknowledgments** The authors state that this work has not received any funding.

**Compliance with ethical standards**

**Conflict of interest** The authors declare that they have no conflict of interest.

## References:

1. Lopez-Beltran A, Scarpelli M, Montironi R, Kirkali Z (2006) 2004 WHO classification of the renal tumors of the adults. Eur Urol 49:798–805
2. Winarti NW, Argani P, De Marzo AM, Hicks J, Mulyadi K (2008) Pediatric renal cell carcinoma associated with Xp11.2 translocation/TFE3 gene fusion. Int J Surg Pathol 16:66–72
3. Haudebourg J, Hoch B, Fabas T, et al. (2010) A novel case of t(X;1)(p11.2;p34) in a renal cell carcinoma with TFE3 rearrangement and favorable outcome in a 57-year-old patient. Cancer Genet Cytogenet 200:75–78
4. Kato H, Kanematsu M, Yokoi S, et al. (2011) Renal cell carcinoma associated with Xp11.2 translocation/TFE3 gene fusion: radiological findings mimicking papillary subtype. J Magn Reson Imaging 33:217–220
5. Liu C, Zhang W, Song H (2017) Nephron-sparing surgery in the treatment of pediatric renal cell carcinoma associated with Xp11.2 translocation/ TFE3 gene fusions. J Pediatr Surg 52:1492–1495
6. Sukov WR, Hodge JC, Lohse CM, et al. (2012) TFE3 rearrangements in adult renal cell carcinoma: clinical and pathologic features with outcome in a large series of consecutively treated patients. Am J Surg Pathol 36:663–670
7. Zhu QQ, Wang ZQ, Zhu WR, Chen WX, Wu JT (2013) The multislice CT findings of renal carcinoma associated with XP11.2 translocation/TFE gene fusion and collecting duct carcinoma. Acta Radiol 54:355–362
8. He J, Huan Y, Qiao Q, Zhang J, Zhang JS (2014) Renal carcinomas associated with Xp11.2 translocations: are CT findings suggestive of the diagnosis? Clin Radiol 69:45–51
9. He J, Gan W, Liu S, et al. (2015) Dynamic computed tomographic features of adult renal cell carcinoma associated with xp11.2 translocation/TFE3 gene fusions. J Comput Assist Tomogr 39:730–736
10. Woo S, Kim SY, Lee MS, et al. (2015) MDCT findings of renal cell carcinoma associated with Xp11.2 translocation and TFE3 gene fusion and papillary renal cell carcinoma. AJR Am J Roentgenol 204:542–549
11. Chen X, Zhu Q, Li B, et al. (2017) Renal cell carcinoma associated with Xp11.2 translocation/TFE gene fusion: imaging findings in 21 patients. Eur Radiol 27:543–552
12. Dang TT, Ziv E, Weinstein S, et al. (2012) Computed tomography and magnetic resonance imaging of adult renal cell carcinoma associated with Xp11.2 translocation. J Comput Assist Tomogr 36:669–674
13. Liu K, Xie P, Peng W, Zhou Z (2014) Renal carcinomas associated with Xp11.2 translocations/TFE3 gene fusions: Findings on MRI and computed tomography imaging. J Magn Reson Imaging 40:440–447
14. Argani P, Lal P, Hutchinson B, et al. (2003) Aberrant nuclear immunoreactivity for TFE3 in neoplasms with TFE3 gene fusions: a sensitive and specific immunohistochemical assay. Am J Surg Pathol 27:750–761
15. Kim SH, Choi Y, Jeong HY, et al. (2011) Usefulness of a break-apart FISH assay in the diagnosis of Xp11.2 translocation renal cell carcinoma. Virchows Arch 459:299–306
16. Rao Q, Shen Q, Xia Q, et al. (2015) PSF/SFPQ Is a very common gene fusion partner in TFE3 rearrangement–associated perivascular epithelioid cell tumors (PEComas) and melanotic Xp11 translocation renal cancers. Am J Surg Pathol 39:1181–1196
17. Verma SK, Mitchell DG, Yang R, et al. (2010) Exophytic renal masses: angular interface with renal parenchyma for distinguishing benign from malignant lesions at MR imaging. Radiology 255:501–507
18. Gurel S, Narra V, Elsayes KM, et al. (2013) Subtypes of renal cell carcinoma: MRI and pathological features. Diagn Interv Radiol 19:304–311
19. Kim Y, Sung DJ, Sim KC, et al. (2017) Renal tumors with low signal intensities on T2-weighted MR image: radiologic-pathologic correlation. Abdom Radiol 42:2108–2118
20. Razek AA, Farouk A, Mousa A, Nabil N (2011) Role of diffusion-weighted magnetic resonance imaging in characterization of renal tumors. J Comput Assist Tomogr 35:332–336
21. Lassel EA, Rao R, Schwenke C, Schoenberg SO, Michaely HJ (2014) Diffusion-weighted imaging of focal renal lesions: a meta-analysis. Eur Radiol 24:241–249
22. He J, Zhou K, Zhu B, et al. (2015) Dynamic contrast-enhanced CT characterization of Xp11.2 translocation/TFE3 gene fusions versus papillary renal cell carcinomas. Biomed Res . https://doi.org/10.1155/2015/298679
23. Raman SP, Johnson PT, Allaf ME, Netto G, Fishman EK (2013) Chromophobe renal cell carcinoma: multiphase MDCT enhancement patterns and morphologic features. AJR Am J Roentgenol 201:1268–1276

24. Hakim SW, Schieda N, Hodgdon T, et al. (2016) Angiomyolipoma (AML) without visible fat: Ultrasound, CT and MR imaging features with pathological correlation. Eur Radiol 26:592–600
25. Wang W, Ding J, Li Y, et al. (2014) Magnetic resonance imaging and computed tomography characteristics of renal cell carcinoma associated with Xp11.2 translocation/TFE3 gene fusion. Plos ONE 9:e99990. https://doi.org/10.1371/journal.pone.0099990
26. Young JR, Coy H, Kim HJ, et al. (2017) Performance of relative enhancement on multiphasic MRI for the differentiation of clear cell renal cell carcinoma (RCC) from papillary and chromophobe RCC subtypes and oncocytoma. AJR Am J Roentgenol 208:812–819
27. Liu N, Wang Z, Gan W, et al. (2016) Renal cell carcinoma associated with xp11.2 Translocation/TFE3 gene fusions: clinical features, treatments and prognosis. PLoS ONE 11:e166897. https://doi.org/10.1371/journal.pone.0166897
28. Egbert ND, Caoili EM, Cohan RH, et al. (2013) Differentiation of papillary renal cell carcinoma subtypes on CT and MRI. AJR Am J Roentgenol 201:347–355
29. Dodelzon K, Mussi TC, Babb JS, Taneja SS, Rosenkrantz AB (2012) Prediction of growth rate of solid renal masses: utility of MR imaging features–preliminary experience. Radiology 262:884–893
30. Haramis G, Mues AC, Rosales JC, et al. (2011) Natural history of renal cortical neoplasms during active surveillance with follow-up longer than 5 years. Urology 77:787–791